EFFECT OF EXTRUSION PROCESS ON THE STRESS CORROSION CRACKING RESISTANCE OF 7N01 ALUMINUM ALLOY

H. Xie [a, b], Z. Yang [b], Q.-S. Ma [b], W. Meng [b], L. Hu [b], X.-H. Yin [b,*]

[a] Key Laboratory of Green Fabrication and Surface Technology of Advanced Metal Materials, Anhui University of Technology, Ministry of Education, Ma'anshan, China
[b] School of Materials Science and Engineering, Anhui University of Technology, Ma'anshan, Anhui, China

Abstract

In this work, the effect of extrusion process on the mechanical properties and the stress corrosion cracking (SCC) resistance of 7N01 aluminum alloys were systematically investigated by tensile testing, slow strain rate testing (SSRT), electrochemical experiment, scanning electron microscopy (SEM), electron backscattered diffraction (EBSD), and transmission electron microscope (TEM) observation, respectively. The results showed that with the increase of extrusion temperature, the SCC resistances of the alloys deteriorated, and this tendency was also proved by the electrochemical experiments including polarization curves and EIS results. The Microstructure observation results revealed that recrystallization played an important role on the SCC resistances of the alloys: the new recrystallization grain boundaries with higher grain boundary energy and wider PFZ could magnify the difference of electrochemical property between grain boundary area and the grain interior, thus raising the stress corrosion crack sensitivity of the alloys.

1. Introduction

Due to its good weldability and high strength, the Al-Zn-Mg alloys have attracted considerable interests in aerospace and transportation industry in the past several decades [1-4]. As one of the typical Al-Zn-Mg alloys with medium-strength, the A7N01 aluminum alloy has excellent extrusion performance, and is being increasingly used in the railway train body structures [5]. However, due to the lack of copper element, the corrosion resistance of the Al-Zn-Mg alloys is not ideal, thus several heat treatments such as retrogression and re-aged (RRA) and multi-step overaged have been developed in order to overcome the stress corrosion cracking (SCC) problem of Al-Zn-Mg alloys [6-8].

For Al-Zn-Mg-(Cu) alloys, solution treatment plays an important role because it directly affects the final mechanical properties and corrosion properties of the alloys [9]. As a vehicle body structural material, the 7N01 profile size has a length of up to 25 meters, thus the solution treatment can only be completed online on the extrusion beltline [10]. Due to the absence of special solution treatment step, the deformation structures formed in the hot extrusion process are preserved in the final state sample, which may directly affect the corrosion properties. Thus, it is essential to study the effort of hot extrusion process on the SCC resistance of 7N01 aluminum alloy. However, relatively little research has been made on the effect of processing technology on the SCC susceptibility of Al-Zn-Mg alloy which is with on-line solution-quench treatment.

Hot extrusion process would directly affect the recrystallization situation of the aluminum alloy [11]. Some researchers have reported the recrystallization effort on the SCC susceptibility of Al-Zn-Mg alloy [12-14]. Huang et.al reported that the inter-granular corrosion resistance of partially recrystallized 7xxx aluminum alloy sheet was better than that of fully recrystallized plate by the investigation of the influence of rolling parameters on the inter-granular corrosion behavior of 7475 aluminum alloy [15]. Deng et.al reported that Sc and Zr microalloying addition could observably improve the corrosion properties of 7xxx aluminum alloys by inhibiting the recrystallization process [16].

In this paper, the mechanical properties and the corrosion susceptibilities of 7N01 alloys under different extrusion temperature in T5 condition were comparatively investigated. The aim of this study was to build the relationship between extrusion process, recrystallization, and the stress corrosion cracking behavior.

2. Experimental

Table 1 shows the chemical compositions of 7N01 aluminum alloys by inductively coupled plasma mass spectrometer (ICP-MS, Nex ION 2000G) method. The alloys were cast by semi-continuous chill casting and cast into an iron mold with internal dimensions of 50 mm. After being homogenized at 470 °C for 24 hours, the ingots were processed into a round bar with the size of Φ49*150 mm for extrusion. The samples were extruded on a four-column hydraulic press using a die and a small extrusion barrel. Samples and extrusion die were incubated at 460-520 °C and 420 °C for 1 h, respectively. Graphite and oil were used as lubricant during the extrusion process. The extruded bars were cooled by water spray quenching and placed in a hot blast drying oven for T5 state peak aging treatment (120 °C/48 h). The sample numbers and extrusion process parameters are listed in Table 2.

Tensile properties were conducted on a MTS810 universal testing machine with 2 mm/min loading speed, and all test data were obtained by three parallel samples. SCC susceptibility was evaluated using the slow strain rate test (SSRT) according to the specification of GB 15970.7-2000 with the strain rates of 5×10^{-6} s^{-1}. The long axis of the specimen was perpendicular to the extrusion direction. Some specimens were tested in air, while for other specimens, the gauge sections were completely immersed in an aqueous 3.5% NaCl solution during the whole testing. The sample size for SSRT is shown in Fig.1. Electrochemical experiments were carried out using the three-electrode system with Pt conducted as auxiliary electrode and saturated calomel electrodes (SCE)

conducted as reference electrode. The studied alloy of 1×1 cm was prepared as the working electrode, and the tests ranged from -1.3 V to -0.5 V with a scan rate of 1 mV/s. Additionally, electrochemical impedance spectroscopy (EIS) tests were conducted at the open circuit potential with a frequency sweep from 0.01 Hz to 100 kHz. The experimental data of the impedance were analyzed using the Zview software, and the values of these parameters were simulated by an equivalent electrical circuit.

The FEI Quanta 200 scanning electron microscopy(SEM) was used to observe the specimen fracture surfaces which test in the Chlorine solution after SSRT. The samples were firstly immersed in the prepared solution and then washed in concentrated HNO_3 (30wt.%), to remove corrosion products. The grain boundary and recrystallization characteristics were studied by Electron backscattered diffraction (EBSD). Specimens for the EBSD and the TEM were mechanically thinned, followed by a twin-jet polishing in the solution of HNO_3:CH_3OH in a ratio of 3:7 at -30 °C. The EBSD samples were examined by FEI Helios nanolab 600i scanning electron microscope (SEM) equipped with an EBSD detector (Oxford, NordlysMax2) operating at 20KV, scanning with a step size of 0.5 μm. And the TEM samples were characterized by Tecnai G2 F20 TEM operating at 200 KV.

3. Results and Discussion
3.1. Tensile properties

Fig.2 shows the tensile properties of the samples. The tensile strength of samples 1#, 2#, 3#, and 4# were 389 MPa, 411 MPa, 416 MPa, and 397 MPa,

Table 1. *Main elemental compositions of the studied alloy (weight fraction, %) by the ICP-MS method*

Materials	Zn	Mg	Cu	Mn	Cr	Zr	Ti	Fe	Si	Al
A7N01	4.35	1.50	0.15	0.34	0.20	0.18	0.09	0.08	0.06	Bal.

Table 2. *Specific extrusion process parameters*

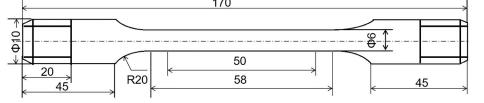| Samples numbers	Ingots temperature /°C	Dies temperature /°C	Holding time /min	Ingot diameter /mm	Bar diameter /mm	Extrusion ratio
1#	460					
2#	480	420	60	49	15.8	9.6
3#	500					
4#	520					

Figure 1. *Schematic illustration of the specimen sampling*

respectively. With the extrusion temperature increase, the yield strength ($\sigma_{0.2}$) and tensile strength (σ_b) of the samples first increased and then decreased, reaching the peak value for 3# sample.

3.2. Stress corrosion behavior

Fig.3 shows the SSRT results of the specimens. We can find that both the strength and elongation of the samples tested in Chlorine solution decreased as compared to the samples tested in air. According to ASTM G129, the Eq. (1) was used to evaluate the SCC susceptibility index, P_{SCC} [17].

$$P_{SCC} = \frac{P_{NaCl}}{P_{air}} \times 100\% \tag{1}$$

where P_{NaCl} and P_{air} were the values of the measured property in NaCl solution and air, respectively. The P_{SCC} values are listed in Table 3, and a higher value suggested better SCC resistance for the samples.

From Table 3, it was clearly indicated that the SCC resistance decreased with the increase of extrusion temperature. It is also found that compared with 1# sample, the SCC resistance of 2# sample decreased slightly, but that of 3# and 4# decreased significantly.

3.3. Polarization curves

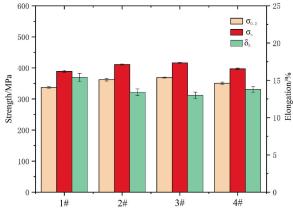Fig.4 shows the typical polarization curves of the

studied samples, and the related electrochemical parameters are listed in Table 4. With the increase of extrusion temperature, corrosion potentials of the alloys decreased, and the corrosion current density increased significantly. According to Faraday's law [18]:

$$K = 3600 \frac{A I_{corr}}{N f} \tag{2}$$

where K is the corrosion rate, F is the Faraday constant, N is the valence number of metal, A is the relative atomic weight, and I is corrosion current density. Hence, the corrosion rate is proportional to the corrosion current density, and larger corrosion
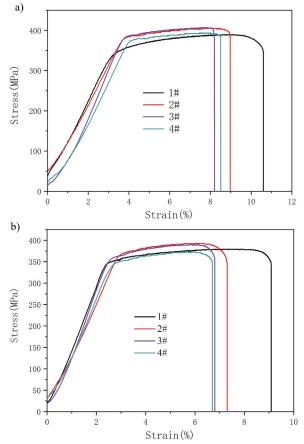
Figure 3. Strain stress curve of SSRT alloys (a) in air and (b) in 3.5%NaCl solution

Figure 2. Tensile mechanical properties of the samples

Table 3. Results of SSRT for the specimens subjected to various extrusion process parameters

	Environment	YS /MPa	YS$_{SCC}$ /%	UTS /MPa	UTS$_{SCC}$ / %	TE / %	TE$_{SCC}$ / %
1#	air	338	98.2	390	97.2	10.6	85.85
	3.5%Nacl	332		379		9.1	
2#	air	377	95.2	405	97.0	9.0	84.27
	3.5%Nacl	359		393		7.3	
3#	air	378	92.9	407	95.8	8.2	82.92
	3.5%Nacl	351		390		6.8	
4#	air	364	90.7	394	94.7	8.5	78.82
	3.5%Nacl	330		373		6.7	

current density implies faster corrosion rate. Meanwhile, more negative corrosion potential leads to stronger corrosion tendency [19]. Therefore, it can be concluded that with the increase of extrusion temperature, the corrosion properties of the alloys deteriorated. This trend was consistent with the results of the slow strain test results.

3.4. EIS

The EIS results as Nyquist and Bode-phase data are shown in Fig. 5, and the corresponding values are listed in Table 5. For Fig. 5a, the impedance curves of 1# and 2# revealed Warburg impedance in the low-frequency region and a capacitive reactance arc in high-frequency region. However, the impedance curves of 3# and 4# showed nearly completed arcs. For Fig. 5a, it was shown that the radius of capacitive arc increased with the increasing of extrusion temperature. According to the result of Xiao et al., the

radius of capacitive arc was closely related to the charge transfer resistance of corroded electrode, and a smaller radius meant a smaller transfer resistance and a faster corrosion reaction rate [20]. Meanwhile, the decrease of the height and width of the maximum phase angle also suggested the decrease of the charge transfer resistance with the increasing extrusion temperature [21].

The electrochemical process was simulated using a Zsimpwin software in Fig. 5c and the corresponding values are listed in Table 5, where Rs represents the solution resistance; R_{ct} and R_{po} represent the charge transfer resistance [22]. Since it hardly had pure capacitance in real electrochemical behavior, a constant phase element (CPE) was always used to
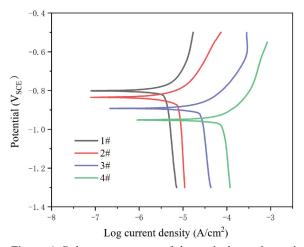
Table 4. *Electrochemical parameters obtained from I/E Tafel slope analyses in Fig.4 (β_c is the cathodic slope and β_a is anodic slope, respectively)*

	Corrosion potential Ecorr /V	Corrosion current density I_{corr} /(A/cm^2)	β_a (mVdec-1)	β_c (mVdec-1)
1#	-0.802	3.954*10^{-6}	229	-1894
2#	-0.835	7.962*10^{-6}	339	-3451
3#	-0.893	2.472*10^{-5}	212	-1792
4#	-0.950	7.638*10^{-5}	184	-1688

Figure 4. *Polarization curves of the studied samples and the electrochemical parameters*
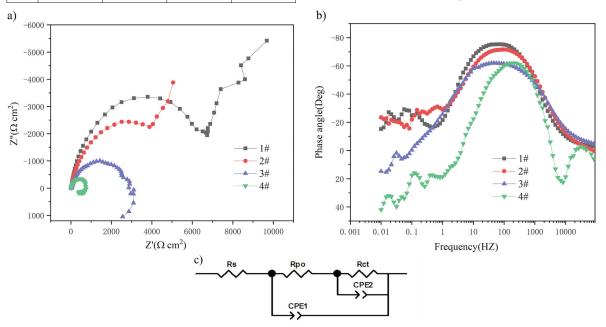
a)

b)

c)

Figure 5. *(a) Nyquist plots, (b) Bode plots, and (c) equivalent circuit used to fit the behavior of samples in 3.5% NaCl solution*

obtain a more accurate fit to the experimental results [23]. According to the reports by Liu et al., the total resistance R_{ct} (neglecting the solution resistance R_s which was almost constant in all cases) was inversely proportional to the corrosion rate [24]. For this study in Table 5, the values of R_{ct} decreased rapidly with the increasing of the extrusion temperature. Thus, it can be concluded that the corrosion properties of the alloys deteriorated with the increase of extrusion temperature.

3.5. SEM observation of the fracture surfaces

Representative fracture surfaces (from the SSRT tests in 3.5% NaCl solution) of the samples are showed in Fig. 6. The fractograph showed a ductile transgranular nature with copious dimples in Fig. 6a. However, with the increase of extrusion temperature, the number of dimples decreased and some tearing ridges could be observed in Fig.6c. When the

extrusion temperature reached 520 ℃, the dimples disappeared and the fractograph exhibited severe SCC attacks with intergranular fracture (Fig.6d).

3.6. EBSD observation

Fig.7 shows EBSD analysis results and bright-field images of the specimens subjected to various extrusion process parameters (The LD direction represents the extrusion direction). It can be clearly seen that the squeezed grains had the elongated fibrous structures, and partially recrystallized fine grains could be observed at the elongated grain boundaries. Meanwhile, the misorientation angle distribution map in Fig.7e showed that the proportion of large-angle grain boundaries rose with the increasing of extrusion temperature. This indicated that higher extrusion temperature would increase the recrystallization ratio of the samples.

Table 5. *Electrochemical parameters obtained from EIS analysis*

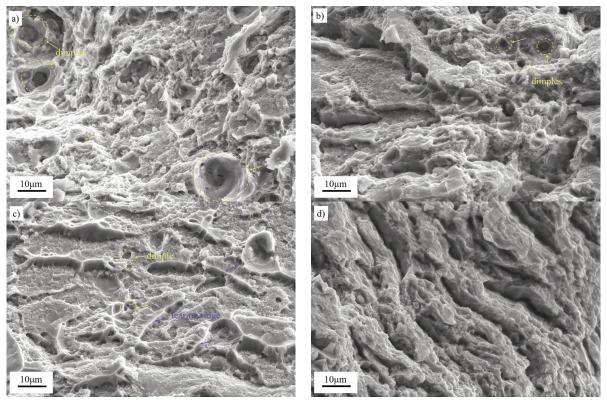|	R_s	$CPE1\text{-}C_1$	$CPE1\text{-}n_1$	R_{po}	$CPE\text{-}C_2$	$CPE2\text{-}n_2$	R_{ct}
1#	22.68	$1.043*10^{-5}$	0.9162	7422	$3.87*10^{-4}$	1.0	$1.258*10^4$
2#	22.01	$1.174*10^{-5}$	0.878	5755	$7.898*10^{-5}$	1.0	8381
3#	10.66	$4.861*10^{-5}$	0.785	780.3	$9.398*10^{-6}$	0.8045	2174
4#	7.147	$4.216*10^{-7}$	1	34.8	$2.02*10^{-6}$	0.9239	688.9

Figure 6. *SEM micrographs of the SCC fracture of the samples failed in 3.5% NaCl solution:*
a) 1#, b) 2#, c) 3# d) 4#

Studies have shown that the corrosion resistance of the grain boundary is closely related to the grain boundary energy, and higher grain boundary energy means the grain boundaries are more easily to crack [25]. The grain boundary energy can be related to the orientation angle [26]:

$$\gamma = \gamma_0 \theta \left(A - \ln \theta \right) \qquad (3)$$

Including, γ_0 is constant, depends on the material's shear modulus G, Poisson's ratio v, and Berber vector b; and θ is grain boundary angle. It showed that the grain boundary energy increased with the grain boundary angle (θ). Apparently, the grain boundary
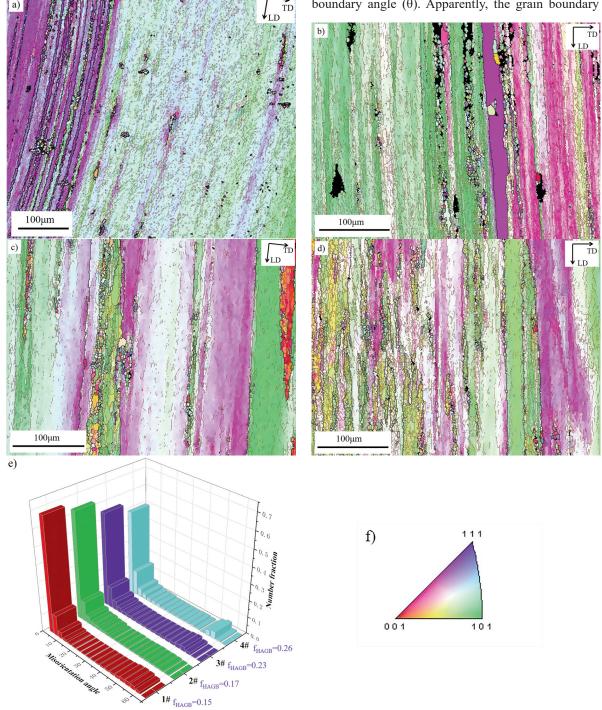

Figure 7. EBSD analysis results and bright-field TEM images of the specimens subjected to various extrusion process parameters: a) 1#, b) 2#, c) 3#, d) 4#; e) misorientation angle distribution, f) representation of the colour code

energy of high-angle grain boundary (HAGB) was much larger than that of the low-angle grain boundary (LAGB) [27]. Therefore, it was easier to crack during the corrosion process [28]. Thus, it can be concluded that with the increase of extrusion temperature, a certain proportion of LGAB was transformed to HAGB. This would weaken the resistance of grain boundaries to corrosion and cause the alloys to change from the original transgranular fracture to intergranular brittle fracture during SSRT, as showed in Fig.6.

3.7. TEM observation

Fig.8 shows the bright-field TEM images of the specimens subjected to various extrusion temperature. In the grain interior, fine and dense precipitates (η' phases) could be observed. With the increase of the extrusion temperature from 460 °C to 500 °C, the precipitation phase structures did not change significantly, only the precipitate free zone (PFZ) seemed to become wider. However, with further increase of the temperature up to 520 °C (4#), the precipitates both in grains interior and grain boundaries coarsened and the number density decreased, resulting in a decline in the overall performance of the alloy. Meanwhile, the width of the PFZ was up to 52 nm.

From the TEM results, it can be seen that the width

of PFZ in the grain boundary become wider with the increase of extrusion temperature. According to the "solute poor theory", higher extrusion temperature meant more thorough solid solution [29]. After aging treatment, the precipitation of equilibrium phases was more sufficient, resulting in the lack of solute atoms near the grain boundary, thus the PFZ became wider [30]. Broad grain boundary precipitation free zone magnified the difference of electrochemical property between the grain boundary interior and grain boundary area, which could promote anodic corrosion reaction [31]. Thus, the corrosion resistance of the alloys was reduced.

Based on the EBSD and TEM results, a model showed schematically in Fig.9 was used to explain the effects of recrystallization on the stress corrosion cracking of Al-Zn-Mg alloys. The proportion of recrystallization increased with the increasing of extrusion temperature, thus there were more numbers of recrystallization grain boundaries on the SCC path. Compared with the sub-grain boundaries in the initial elongated grain, the new recrystallization grain boundaries were high-angle grain boundaries with higher grain boundary energy and wider PFZ which magnified the difference of electrochemical performance between the grain boundary interior and grain boundary area, thus raising the stress corrosion crack sensitivity of the alloys.
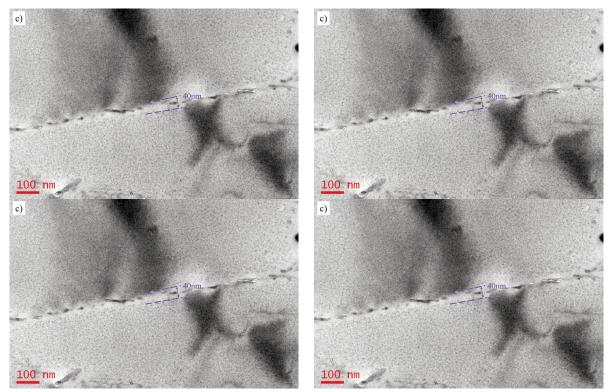

Figure 8. Bright-field TEM images of the specimens subjected to various extrusion process parameters: a)1#, b) 2#, c) 3#, d) 4#
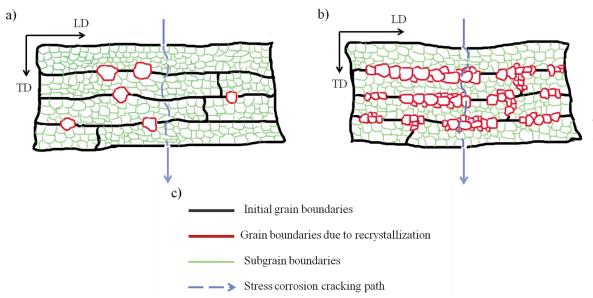
Figure 9. Schematic depiction of SCC propagation on the grain structure with a) extrusion microstructure with few recrystallized grain; b) with significant amounts of recrystallization grains; c) meaning of the symbols

4. Conclusion

In summary, the mechanical properties and the SCC susceptibilities of the 7N01 alloy with different extrusion temperature are investigated. With the increase of extrusion temperature, the stress corrosion properties of the alloy deteriorated, and this tendency was also proved by the electrochemical experiments results which included polarization curves and EIS. The fractograph showed that with the increase of extrusion temperature, the fracture morphology which tested in chlorine solution changed from brittle inter-granular fracture into ductile transgranular fracture. Microstructure observation results revealed that recrystallization played an important role on the SCC resistances of the alloys: the new recrystallization grain boundaries with higher grain boundary energy and wider PFZ could magnify the difference of electrochemical performance between the grain boundary interior and grain boundary area, thus raising the SCC sensitivity of the alloys.

Author contributions

HX: Performed the experiments and wrote the original draft; ZY: Performed the analysis with constructive discussions; QSM and WM: Data curation; LH: Writing—review & editing; XHY: Analyzed the results and revised the original draft;

Data availability Statement

The raw/processed data required to reproduce these findings cannot be shared at this time as the data also forms part of an ongoing study.

Conflict of interest:

The authors declare that they have no known competing financial interests or personal relationships that could have appeared to influence the work reported in this paper.

References

[1] T. Engdahl, V. Hansen, P.J. Warren, K. Stiller, Investigation of fine scale precipitates in Al-Zn-Mg alloys after various heat treatments, Materials Science and Engineering A, 327 (2002) 59–64. https://doi.org/10.1016/S0921-5093(01)01876-7

[2] J.C. Williams, E.A. Starke Jr, Progress in structural materials for aerospace systems, Acta Materialia, 51 (2003) 5775–5799. http://dx.doi.org/10.1016/j.actamat.2003.08.023

[3] H. R. Zaid, A. M. Hatab, A. M. A. Ibrahim, Properties enhancement of Al-Zn-Mg alloy by retrogression and re-aging heat treatment, Journal of Mining and Metallurgy Section B: Metallurgy, 47 (1) (2011) 31-35. https://doi.org/10.2298/JMMB1101031Z

[4] P. K. Rout, M.M. Ghosh, K.S. Ghosh, Microstructural, mechanical and electrochemical behaviour of a 7017 Al–Zn–Mg alloy of different tempers, Materials Characterization, 104 (2015) 49-60. http://dx.doi.org/10.1016/j.matchar.2015.03.025

[5] H. Xie, Z. Xiao, Z.Li, M.P. Wang, S. Ma, H.Y Jiang, Quench sensitivity of AA7N01 alloy used for high-speed train body structure, JOM, 71(5) (2019) 1681-

1686. https://doi.org/10.1007/s11837-018-3162-z

[6] S. Li, H.G Dong, P. Li, S. Chen, Effect of repetitious non-isothermal heat treatment on corrosion behavior of Al-Zn-Mg alloy, Corrosion Science, 131 (2018) 278-289. https://doi.org/10.1016/j.corsci.2017.12.004

[7] H. Xie, L. Hu, Q.-H. Ma, W. Meng, X.-H. Yin, Microstructure and mechanical properties of A7N01 aluminum alloy weld joints filled with ER5356 and ER5087 weld wires, Journal of Mining and Metallurgy Section B: Metallurgy, 58 (1) (2022) 157-167. https://doi.org/10.2298/JMMB210625056X

[8] Y. Reda, R. Abdel-Karim, I. Elmahallawi, Improvements in mechanical and stress corrosion cracking properties in Al-alloy 7075 via retrogression and reaging, Materials Science and Engineering A, 485 (2008) 468–475. https://doi.org/10.1016/j.msea.2007.08.025

[9] S.Y. Chen, K.H. Chen, G.S. Peng, H.C. Fang, Effects of solution temperature on microstructure and stress corrosion of Al-Zn-Mg-Cu aluminum alloy, Materials Science and Engineering of Powder Metallurgy, 15(5) (2010) 456-462. https://doi.org/10.3969/j.issn.1673-0224.2010.05.008

[10] X.M. Wang, B. Li, M.X. Lia, H.G. Cui, H. Chen, Study of local-zone microstructure, strength and fracture toughness of hybrid laser-metal-inert-gas-welded A7N01 aluminum alloy joint, Materials Science and Engineering A, 688 (2017) 114–122. https://doi.org/10.1016/j.msea.2017.01.087

[11] H. Tanaka, H. Esaki, K. Yamada, K. Shibue, H. Yoshida, Improvement of mechanical properties of 7475 based aluminum alloy sheets by controlled warm rolling, Materials Transactions, 45(1) (2004) 69-74. https://doi.org/10.2320/matertrans.45.69

[12] J.T. Jiang, W.Q. Xiao, L. Yang, W.Z. Shao, S.J. Yuan, L. Zhen, Ageing behavior and stress corrosion cracking resistance of anon-isothermally aged Al–Zn–Mg–Cu alloy, Materials Science and Engineering A, 605 (2014) 167–175. https://doi.org/10.1016/j.msea.2014.03.023

[13] L.Q. Xie, Q. Lei, M.P. Wang, X.F. Sheng, Z. Li, Effects of aging mechanisms on the exfoliation corrosion behavior of a spay deposited Al-Zn-Mg-Cu-Zr aluminum alloy, Journal of Materials Research, 32 (2017) 1105-1117. https://doi.org/10.1557/jmr.2017.64

[14] X.Y. Sun, B.Zhang, H.Q. Lin, Y. Zhou, L.Sun, J.Q. Wang, E.H. Han, W. Ke, Correlations between stress corrosion cracking susceptibility and grain boundary microstructures for an Al-Zn-Mg alloy, Corrosion Science, 77 (2013) 103-112. https://doi.org/10.1016/j.corsci.2013.07.032

[15] M.C. Huang, Effect of grain structure on intergranular corrosion resistance of 7475 aluminum alloy, Mining and Metallurgical Engineering, 30(6) (2010) 97-99. https://doi.org/10.3969/j.issn.0253-6099.2010.06.026

[16] Y. Deng, Z.M. Yin, K. Zhao J.Q. Duan, J. Hu, Z.B. He, Effect of Sc and Zr microalloying additions and aging time at 120°C on the corrosion behaviour of an Al-Zn-Mg alloy, Corrosion Science, 65 (2012) 288-298. https://doi.org/10.1016/j.corsci.2012.08.024

[17] L.L Wei, Q.L. Pan, L. Feng, Effect of aging on corrosion property, electrochemical behavior and microstructure of Al-Zn-Mg-Cu alloy, Materials Corrosion, 66(1) (2015) 54-60.

https://doi.org/10.1002/maco.201307095

[18] D.A. Hardwick, A.W. Thompson, I.M. Bernstein, The effect of copper and heat treatment on the hydrogen embrittlement of 7050-type alloys, Corrosion Science, 28 (1988) 1127-1137. http://dx.doi.org/10.1016/0010-938x(88)90123-0

[19] L.H. Lin, Z.Y. Liu, X.N. Han, W.J. Liu, Effect of overaging on fatigue crack propagation and stress corrosion cracking behaviors of an Al-Zn-Mg-Cu alloy thick plate, Journal of Materials Engineering and Performance, 27 (2018) 3824-3830. https://doi.org/10.1007/s11665-018-3518-0

[20] Y.P. Xiao, Q.L. Pan W.B Li, X.Y. Liu, Y.B He, Influence of retrogression and re-aging treatment on corrosion behavior of an Al–Zn–Mg–Cu alloy, Materials and Design, 32 (2011) 2149–2156. http://dx.doi.org/10.1016/j.matdes.2010.11.036

[21] A.F. Oliveira, Jr., M.C. de Barros, K.R. Cardoso, D.N. Travessa, The effect of RRA on the strength and SCC resistance on AA7050 and AA7150 aluminium alloys, Materials Science and Engineering A 379 (2004) 321–326. http://dx.doi.org/10.1016/j.msea.2004.02.052

[22] Conde, J. de Damborenea, Electrochemical modelling of exfoliation corrosion behaviour of 8090 alloy, Electrochimica Acta, 43(8), 1998, 849-860. http://dx.doi.org/10.1016/S0013-4686(97)00218-1

[23] T.C. Tsai, T.H Chuang, Role of grain size on the stress corrosion cracking of 7475 aluminum alloys, Materials Science and Engineering A, 225 (1997) 480–490. http://dx.doi.org/ 10.1016/S0921-5093(96)10840-6

[24] J.C. Liu, S. Park, S. Nagao, M. Nogi, H. Koga, J.S. Ma, G. Zhang, K. Suganuma, The role of Zn precipitates and Cl⁻ anions in pitting corrosion of Sn-Zn solder alloys, Corrosion Science, 92 (2015) 263-271. https://doi.org/10.1016/j.corsci.2014.12.014

[25] S.Y. Chen, K.H. Chen, P.X. Dong, S.P. Ye, L.P. Huang, Effect of recrystallization and heat treatment on strength and SCC of an Al-Zn-Mg-Cu alloy, Journal of Alloys and Compounds, 581 (2013) 705-709. http://dx.doi.org/ 10.1016/j.jallcom.2013.07.177

[26] T. Minoda, H. Yoshida, Effect of grain boundary characteristics on intergranular corrosion resistance of 6061 aluminum alloy extrusion, Metallurgical and Materials Transactions A, 33 (2003) 2891-2898. https://doi.org/10.1007/s11661-002-0274-3

[27] X. Huang, Q.L. Pan, B. Li, Z.M. Liu, Z.Q. Huang, Z.M. Yin, Microstructure, mechanical properties and stress corrosion cracking of Al-Zn-Mg-Zr alloy sheet with trace amount of Sc, Journal of Alloys and Compounds, 650 (2015) 805-820. http://dx.doi.org/10.1016/j.jallcom.2015.08.011

[28] H.C. Fang, H. Chao, K.H. Chen, Effect of recrystallization on intergranular fracture and corrosion of Al-Zn-Mg-Cu-Zr alloy, Journal of Alloys and Compounds, 622 (2015) 166-173. http://dx.doi.org/10.1016/j.jallcom.2014.10.044

[29] A.Aytac, B. Dascilar, M. Usta, The effect of extrusion speed on the structure and corrosion properties of aged and non-aged 6063 aluminum alloy, Materials Chemistry and Physics, 130 (2011) 1357-1360. http://dx.doi.org/ 10.1016/j.matchemphys.2011.09.029

[30] H.C Fang, F.H Luo, K.H. Chen, Effect of intermetallic phases and recrystallization on the corrosion and fractrure behavior of an Al-Zn-Mg-Cu-Zr-Yb-Cr alloy, Materials Science and Engineering A, 684 (2017) 480–490. http://dx.doi.org/10.1016/j.msea.2016.12.009

[31] Y. Deng, R. Ye, G.F. Xu, J.D. Yang, Q.L. Pan, B. Peng, X.W. Cao, Y.L. Duan, Y. J. Wang, L.Y. Lu, Z.M. Yin, Corrosion behaviour and mechanism of new aerospace Al–Zn–Mg alloy friction stir welded joints and the effects of secondary $Al_3Sc_xZr_{1-x}$ nanoparticles, Corrosion Science, 90 (2015) 359-374. http://dx.doi.org/10.1016/j.corsci.2014.10.036

EFEKAT POSTUPKA EKSTRUZIJE NA OTPORNOST LEGURE ALUMINIJUMA 7N01 NA PUCANJE OD KOROZIJE POD NAPONOM

H. Xie [a, b], Z. Yang [b], Q.-S. Ma [b], W. Meng [b], L. Hu [b], X.-H. Yin [b,*]

[a] Glavna laboratorija za zelenu izradu i tehnologiju naprednih materijala, Tehnološki univerzitet u Anhueju, Ministarstvo obrazovanja, Ma'anšan, Kina
[b] Fakultet za nauku i inženjerstvo materijala, Tehnološki univerzitet u Anhueju, Ministarstvo obrazovanja, Ma'anšan, Kina

Apstrakt

U ovom radu su sistematski ispitani efekti postupka ekstruzije na otpornost legure aluminijuma 7N01 na pucanje od korozije pod naponom (SCC). Ispitivanje je obuhvatalo ispitivanje naprezanja, ispitivanje sporog stepena deformacije, elektrohemijski eksperiment, SEM, EBSD i TEM analizu. Rezultati su pokazali da se otpornost na SCC kod legure pogoršala sa povećanjem temperature ekstruzije, što je potvrđeno i elektrohemijskim eksperimentima koji su uključivali i krive polarizacije i rezultate EIS. Rezultati posmatranja mikrostrukture su pokazali da rekristalizacija igra važnu ulogu kod otpornosti na SCC: nove granice rekristalizacije kod zrna sa većom energijom granice zrna i širim područjem precipitacione faze mogu povećati razliku u elektrohemijskim svojstvima između područja granica zrna i unutrašnjosti zrna, čime se povećava osetljivost na pucanje od korozije pod naponom.

Ključne reči: *Pucanje od korozije pod naponom; Postupak ekstruzije; Rekristalizacija; Al-Zn-Mg legure*